Available online at www.sciencedirect.com
SCIENCE DIRECT®
ELSEVIER
Global and Planetary Change 37 (2003) 33–56
GLOBAL AND PLANETARY CHANGE
www.elsevier.com/locate/gloplacha

Influence of North American land processes on North Atlantic Ocean variability

Uma S. Bhatt[a,*], Edwin K. Schneider[b], David G. Dewitt[c]

[a] *International Arctic Research Center/Frontier, University of Alaska-Fairbanks, 930 Koyukuk Drive, P.O. Box 75-7335, Fairbanks, AK 99775-7335, USA*
[b] *Center for Ocean Land Atmosphere Studies, Calverton, MD, USA*
[c] *International Research Institute, Palisades, NY, USA*

Received 20 June 2001; accepted 6 July 2002

Abstract

A set of numerical simulations has been carried out to evaluate the influence of coupled land–atmosphere and ocean–atmosphere interactions on natural climate variability. The baseline experiment was a long integration of a state-of-the-art-coupled atmosphere–ocean–land general circulation model (GCM). A sensitivity experiment was conducted in which the ocean and atmosphere were fully interactive but the soil moisture was specified. This paper describes a connection found between land–atmosphere coupling and midlatitude sea surface temperature (SST) variability in the North American–North Atlantic sector.

Specifying soil moisture results in a reduction in surface and atmospheric temperature variability and also an increase in net heat flux variability. Surface temperature variance is reduced because it is constrained by the fixed soil moistures. Since the surface temperature cannot equilibrate with a given atmospheric anomaly, the resulting heat flux will be quite large and will act to damp the atmospheric anomaly. This is consistent with larger heat flux variance and reduced temperature variance in the simulation with suppressed land processes.

SST anomalies in the midlatitude Atlantic are sensitive to air temperature and moisture anomalies modified over the North American continent, so it is not unexpected that SST variance is significantly reduced when land temperature variability decreases. Oceanic 're-emergence' operates in both simulations but is weaker in the fixed soil moisture integration, particularly in a region of the western North Atlantic contiguous with North America. Reemergence is the mechanism by which late winter ocean temperature anomalies are sequestered below the stable summer ocean mixed layer and reentrained into the deepening autumn mixed layer. The larger oceanic anomalies in the fully coupled simulation decay more slowly and are a partial explanation for stronger reemergence. However, during the second winter, the atmospheric forcing favors the same sign of SST anomalies as those reemerging and, therefore, acts to reinforce the anomalies in the fully coupled simulation.

An area averaged SST index was constructed for the region of the western North Atlantic where reemergence was most notably reduced. This index was used to construct composites which suggest that, in the fully coupled model, land surface temperature and SST anomalies both reemerge the second winter, whereas in the suppressed land processes simulation, there is no

* Corresponding author.
E-mail address: bhatt@iarc.uaf.edu (U.S. Bhatt).

doi:10.1016/S0921-8181(02)00190-X

winter-to-winter reappearance of land surface temperature anomalies. The late winter land temperatures are able to reemerge in fall because of the persistence of soil moisture anomalies.

Keywords: land processes; general circulation model; North America

1. Introduction

A better understanding of how the components of the climate system influence the low frequency variability has long been of practical interest for seasonal climate forecasting. Namias (1959) hypothesized that soil moisture played such a role. Namias (1963) demonstrated that dry spring conditions over North America associated with enhanced 700 mb anticyclonic circulation are followed by increased sensible heat transfer to the atmosphere, a subsequent warming of the atmosphere which in turn helps to maintain the anticyclonic circulation throughout the summer. Similar arguments can be constructed to explain why a rainy summer is likely to follow a wetter than normal spring. Rind (1982), using a coarse general circulation model and a simple two-layer representation of soil moisture, found that summertime climate was better predicted when spring ground moisture anomalies were known. Delworth and Manabe (1989) conducted a pair of multiyear experiments with the GFDL general circulation model with predicted and specified soil moistures. They found that the persistence in soil moisture acts to increase the variability and persistence of midlatitude summertime relative humidity and air temperature. Strong persistence and large spatial correlations of observed soil moisture measured in central Russia have been documented by Vinnikov et al. (1996). Examining a 10-year coupled land–atmosphere GCM integration, Liu and Avissar (1999) find that soil moisture plays a more significant role in adding persistence to the climate than soil temperature. Huang et al. (1996) demonstrated that soil moisture provides skill in predicting air temperatures over the continental United States, particularly at long leads. These modeling studies and others (Koster and Suarez, 1995; Betts et al., 1996) add to the growing body of evidence that support and further refine our understanding of the role of soil moisture in climate variability.

The role of the oceans in interannual climate variability has been studied more extensively. Namias and Born (1970, 1974) observed the tendency for midlatitude SST anomalies to be correlated from one winter to the next without persisting through the intervening summer. They proposed a mechanism, termed reemergence by Alexander and Deser (1995). Ocean mixed layer temperature anomalies during late winter penetrate through a deep layer of the ocean and persist through the summer under the stable mixed layer. In the subsequent fall months, as the mixed layer deepens, the temperature anomalies from the previous winter are reincorporated into the upper ocean layer. This mechanism has been investigated using ocean weathership observations and a mixed layer ocean model by Alexander and Deser (1995). Bhatt et al. (1998) used a mixed layer ocean model of the North Atlantic coupled to a global atmospheric model and found enhanced variability of near surface air temperature anomalies on interannual time scales as a result of reemergence. Watanabe and Kimoto (2000) have shown that reemergence also has an influence on decadal variability. The evidence suggests that, at the very least, the midlatitude ocean has a subtle impact on the atmosphere by changing the low frequency variability through enhancing the persistence of anomalies.

A set of numerical simulations was carried out to evaluate the influence of coupled land–atmosphere and ocean–atmosphere interactions on internal climate variability. The baseline experiment was a long integration of a state-of-the-art-coupled atmosphere–ocean general circulation model (GCM). Three auxiliary diagnostic simulations were made in which interactions between the subsystems were selectively eliminated. In this research, we focus our analysis on the fully coupled simulation and the sensitivity experiment where the annual cycle of the soil moisture is specified. The influence of land surface processes can be identified by comparing the climate of these two simulations.

Here, we present an analysis that documents the impact of land surface and ocean processes on the internal climate variability, with a focus on the mid-latitudes. In particular, we investigate the following questions:

- How do land processes influence atmospheric and oceanic variabilities?
- Does reemergence operate in this model? If so, how is the nature of reemergence changed due to suppression of soil moisture variability?
- Does soil moisture variability impact year-to-year persistence of climate anomalies?

2. Models and experiment design

This experimental design is adapted from the study of Schneider and Kinter (1994). The major improvements in the current suite of experiments are use of a coupled GCM with a global ocean domain and interactive sea ice; improvement of the coupled model simulation of climate variability, especially coupled air–sea interactions in the tropical Pacific (ENSO); and constraining the monthly mean climatology of all of the diagnostic experiments to be similar to that of the coupled model, in order to give a clean diagnosis of the influences of the land and ocean on the climate variability.

2.1. Models

This version of the Center for Ocean Land Atmosphere (COLA) Studies coupled model has been described in detail in DeWitt and Schneider (1999), and additional information pertaining to earlier versions can be found in Schneider and Kinter (1994), Xue et al. (1991), Kinter et al. (1988), and DeWitt and Schneider (1997). A history of the COLA coupled model that highlights earlier deficiencies and recent improvements is given in DeWitt and Schneider (1999). The new version of the CGCM shows significant improvement in the simulated mean tropical SST as well as the amplitude and structure of the equatorial annual cycle of SST.

2.1.1. Atmospheric and land models

The atmospheric circulation model is the COLA global spectral model with triangular truncation at wave number 30, with 18 unevenly spaced vertical levels using sigma coordinates in the vertical. Solar radiation is parameterized using the formulation of Lacis and Hansen (1974), and terrestrial radiation is based on the work of Harshvardhan et al. (1987). The turbulent closure scheme for subgrid scale exchanges of heat, momentum, and moisture follows Miyakoda and Sirutus (1977) and Mellor and Yamada (1982). The relaxed Arakawa–Schubert scheme of Moorthi and Suarez (1992) was adapted into the COLA coupled model by DeWitt (1996) to parameterize convection. The diagnostic cloud fraction and optical properties parameterizations were modified from those in Schneider and Kinter (1994) following work done at the National Center for Atmospheric Research (NCAR) on the Community Climate Model (Kiehl et al., 1996, 1998) and is described in DeWitt and Schneider (1997). In addition, gravity wave drag is parameterized according to the formulation of Palmer et al. (1986).

The land model is based on the simplified biosphere model (SiB) developed by Sellers et al. (1986) and implemented by Sato et al. (1989). The COLA model incorporates simplifications of SiB developed by Xue et al. (1991) (simplified SiB) which enhances the computational efficiency. A model grid box is assigned 1 of 12 vegetation types (or permanent ice cover), whose physical and morphological properties are specified but vary seasonally. The model had three soil layers of varying depth based on soil type at a particular model grid box: a very thin surface layer (2 cm), a root zone layer (0.2–1.5 m), and a relatively thick deep soil layer (0.3–2.0 m). There is gravitational drainage and diffusion of moisture between soil layers. The vegetation canopy processes include the resistances to evapotranspiration and heat flux, and the effect on the interception loss of moisture in a model grid box. There is water runoff in the model from excess precipitation and drainage of ground water.

Boundary conditions applied at the lower surface of the AGCM include the specification of SST, sea ice extent, and surface albedo of the oceans. The atmospheric boundary condition is the SST predicted by the OGCM plus a spatially dependent, time-independent term that corrects for the spectral truncation error that produces nonzero elevation of the lower boundary of the atmosphere over the ocean (Campana and Kanamitsu, 1987, personal communication). The details of this correction are given in Schneider et al. (1997).

2.1.2. The ocean model

We employ the Geophysical Fluid Dynamics Laboratory (GFDL) modular ocean model (MOM) version 2.0 (Pacanowski, 1995) to represent the ocean component of the coupled model. This model is a finite difference treatment of the primitive equations of motion on the sphere. Nonlinear vertical mixing of heat, salinity, and momentum is modeled according to Pacanowski and Philander (1981). Horizontal mixing of heat and momentum is parameterized using a Laplacian-type horizontal diffusion with constant coefficients of 4×10^7 and 1×10^9 cm^2 s^{-1}, respectively. The penetration of solar radiation below the surface layer in MOM2 is treated following the work of Rosati and Miyakoda (1988). The model includes a simple thermodynamic model for sea ice which is fully described in Schneider and Zhu (1998).

The zonal resolution of the ocean model is 3.0°, while the meridional resolution is highest in the equatorial waveguide (1.0° between 10°S and 10°N) and decreases to 3.0° poleward of 30°. There are 20 layers in the vertical from the surface to a maximum depth of 5700 m and half the layers represent the top 150 m. Realistic basin boundaries and bathymetry for the world oceans are included globally. The upper 10 layers are 15 m thick, while layers 11 and 12 are 32.8 and 66.6 m thick, respectively.

The initial condition for the coupled integration is a state of rest, with temperature and salinity set to climatological January values from the data of Levitus (1982).

2.1.3. Coupling

Software for coupling the AGCM and OGCM is provided as part of MOM2 and the two models exchange daily mean values every 24 h. The OGCM provides SST values to the AGCM and receives surface fluxes of heat, momentum, and fresh water as well as the solar flux from the AGCM. Since the two models have different resolutions, the ocean model SST is averaged over an atmospheric grid box, and the AGCM surface fluxes are linearly interpolated (note they are not modified in any other way) from the atmospheric to the oceanic grid. The coupled model employs a simplified 360-day astronomical year with twelve 30-day months for the solar cycle. Monthly mean (30-day average) diagnostics have been saved for the analysis.

2.2. Simulations and processing

The fully coupled simulation (COU) was integrated for 193 years. An annual cycle of global SST and soil moisture was constructed by averaging the years 89–109. These climatological SSTs and soil moistures were used in subsequent simulations in order to fix ocean and land processes. The model configuration for the experiments discussed in this paper is listed in Table 1. In the fully coupled simulation (COU), the land, atmosphere, and ocean model components are all active. The atmosphere and ocean are active but the land model is not active in the OCN simulation. Therefore, the difference between OCN and COU is that soil wetness is fixed to an annual cycle in the two lower soil layers in the former while the soil wetness is allowed to freely evolve in COU. The OCN simulation was started from initial conditions of January 1, year 99 of COU and was integrated for 82 years. The last 94 years of COU were used in this analysis.

In the OCN experiment, soil moisture was specified for the deep and the root zones, which comprise the lower two soil layers. The upper surface layer soil moisture was permitted to interact with the atmosphere in order to prevent extreme anomalies in precipitation which result from fixing the very thin uppermost layer. Surface temperature was not specified over land, since it was desired that the surface energy budget be satisfied over land. An essential difference between land and ocean is the much smaller land heat capacity. Consequently, the surface temperature over land adjusts rapidly so that the net heat flux is close to zero on climate time scales. The approach of specifying soil moisture allows some control over land, while maintaining this essential contrast between land and ocean properties.

Table 1
Configuration of model experiments

	COU	OCN
Description	interactive ocean interactive land	interactive ocean fixed soil wetness
Total model years	94	82
Years after detrending	73	61
Globally averaged surface temperature drift (°C)	0.17	0.16

Generally, coupled models tend to drift when flux corrections or restoring forces are not employed. Since flux corrections were not included in these simulations, each time series was high pass filtered using a Lanczos filter (Duchon, 1979) at a 20-year cutoff to remove the long-term drift. The model data were also linearly detrended after the filtering to remove a small linear drift. Globally averaged surface temperature drift, defined as the average of the last 20 years minus the first 20 years of a given simulation, is listed in Table 1. The average drift in the COU and OCN simulations is relatively small; however, it can be notably larger at a specific grid point.

Total soil wetness was calculated globally by using the spatially varying soil layer depths and proportionally combining the soil wetness for each layer. For the region of North America and the time scales of interest in this study, the total soil wetness anomalies resemble those of the deepest soil layer.

3. Results and discussion

3.1. Means and variance of climate anomalies

Annual and seasonal means of the standard meteorological variables (temperature, pressure, specific humidity, and surface temperature) from COU and OCN simulations were not identical but were relatively close. The mean surface temperature climatology differed by approximately 0.5–1 °C in the long-term mean. The long-term means of the 1000 mb temperature and specific humidity varied by about 0.5 °C and 0.1 g/kg, respectively. Since these changes were small, we will proceed with the assumption that the mean climatology is the same for all of the simulations.

Observational as well as modeling studies assert that midlatitude coupled ocean–atmosphere variability on interannual time scales (less than approximately 10 years) is controlled primarily by local interactions that occur through surface heat flux anomalies. Bjerknes (1962, 1964) first described the dipole-like anomaly pattern (see Fig. 4A) and demonstrated that North Atlantic SST anomalies on interannual time scales are negatively correlated with local wind speed and result from anomalous local air–sea heat fluxes. These ideas have been refined through subsequent climate investigations. In an observational study of latent and sensible heat fluxes using the Comprehensive Ocean–Atmosphere Data Set (COADS), Cayan (1992) found that since specific humidity and air temperature gradients were large in the midlatitudes, changes in the wind impact the surface heat fluxes the most by changing the air–sea temperature or moisture difference. The contribution to the sensible (latent) heat flux of the mean wind times the anomalous air–sea temperature (humidity) difference was found to be 2.5 (3) times larger than that of the anomalous wind times the mean air–sea temperature (humidity) difference in COADS by Battisti et al. (1995). The ratio for sensible heat flux is comparable in this version of the coupled COLA model. Therefore, we would argue that it is reasonable to focus on the first-order effects of anomalous air temperature and specific humidity on the development of sea surface temperature (SST) anomalies.

The variance of surface temperature, both over land and ocean, is significantly reduced in the simulations that specify soil moisture (Fig. 1). The ratio of COU/OCN November to March standard deviation of surface temperature (Fig. 1) displays values greater than 1 over the land and ocean in the midlatitudes. When the land model is fully operative, the standard deviation is 25–50% larger over North America and up to 300% larger over South America. Additionally, ENSO variability is significantly larger when there is land variability, an intriguing feature we are examining further in another study. The SST variability is larger around 40°N in the midlatitude North Atlantic when land is fully interactive. In the coupled COLA model, this is a region of westerly flow, hinting at a possible downwind effect of what is occurring over the North American landmass. An examination of these standard deviation ratios for other seasons yields similar results.

The variance of 1000 mb air temperature is generally larger in the simulations with fully interactive land processes (not shown) and resembles the patterns seen in Fig. 1. The ratio of the November to March standard deviation of the near surface air temperature for COU/OCN are greater than 1 over most of North America, but are significant (larger than a 25% increase) only in a narrow band centered at 40°N. The standard deviation of 1000 mb specific humidity is consistent with air temperature changes

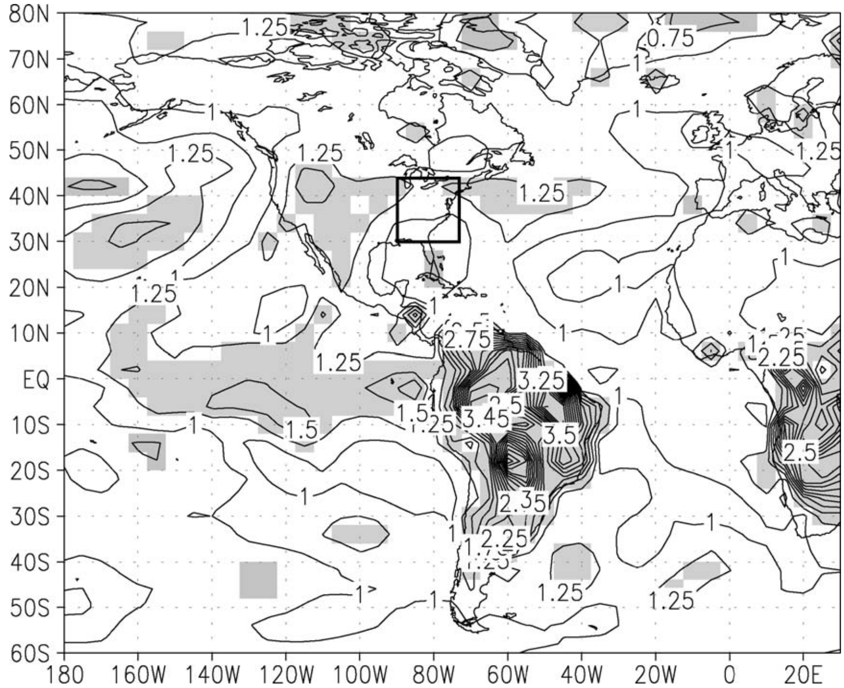

Fig. 1. The ratio of COU/OCN standard deviations of surface temperature seasonally averaged from November to March. Shading signifies statistical significance at 95% or greater level based on an *f*-test. The box over North America (30–45°N and 90–75°W) shows the domain for the time series of 1000 mb temperatures used to construct the autocorrelations in Fig. 3.

and is larger over North America in COU than OCN but is significant only over Mexico and parts of the western US. As with surface temperature, the largest increases in variability in air temperature, and specific humidity occurs over South America and the eastern equatorial Pacific. There is a larger difference between the standard deviation of COU and OCN surface temperature than 1000 mb air temperatures over North America.

Over North America, the variability of total heat flux during November to March is smaller (Fig. 2) by about 25% in the simulations that includes land variability. There are two centers of statistical significance over North America, one in the northeast and the other in the west.

The notion of 'decreased thermal damping' has been applied to air–sea interactions in the midlatitudes (Hasselmann, 1976; Frankignoul, 1985; Barsugli and Battisti, 1998; Bladé, 1997; Bhatt et al., 1998) and appears to have a parallel with air–land interactions in this research. The near surface air temperature variability is larger in a simulation that has an interactive ocean, even using a simple slab (Barsugli and Battisti, 1998, Saravanan, 1998) or a variable depth mixed layer model (Bhatt et al., 1998), than when SSTs are specified. Starting with the notion that the atmosphere is forcing the ocean in the midlatitudes (Wallace and Jiang, 1987), a given air temperature anomaly will force an SST anomaly. When SSTs are fixed, the ensuing heat flux anomaly will be large because of the large temperature differences between the ocean and the atmosphere, and will quickly damp the atmospheric temperature anomaly. However, when the ocean is able to adjust, the resulting heat flux is smaller (smaller air–sea contrast), and this results in a slower damping of air temperature anomalies. Similarly over the midlatitude land, surface temperature variance is reduced since it is constrained by the fixed soil moistures. Consequently, the surface temperature cannot equilibrate with a given atmospheric anomaly, and the resulting large heat flux anomaly will act to quickly damp the atmospheric anomaly. A reduction in heat flux variability and an enhancement of air temper-

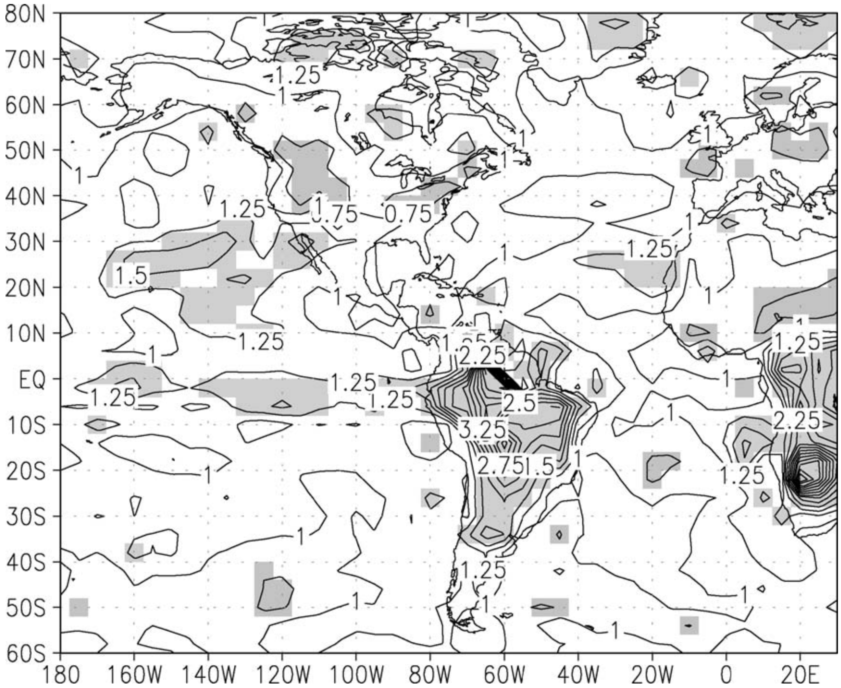

Fig. 2. The ratio of COU/OCN standard deviations of total surface heat flux averaged from November to March. Shading signifies statistical significance at 95% or greater level based on an *f*-test.

ature variability seen over North America (Figs. 1 and 2) is consistent with this notion of 'decreased thermal damping' and suggests an increased persistence of air temperature anomalies when the land is fully interactive. Note in the tropics, the variability of both near surface air temperatures and heat fluxes is larger for COU than OCN. Decreased thermal damping is predicated on the notion that the atmosphere forces the surface, and this is not the case in the tropics where the ocean (or land) forces the atmosphere when considering turbulent heat fluxes.

3.2. Interannual climate variability

The persistence of 1000 mb air temperature and surface temperature over North America in COU is not notably different than that of OCN on monthly time scales. However, there are significant correlations of winter-to-winter and summer-to-summer air and surface temperature anomalies. Monthly autocorrelations of area averaged 1000 mb air temperature over North America (30–45°N and 90–80°W) that start in each month and are lagged from 0 to 14 months are presented in Fig. 3 for the COU and OCN simulations. Shading indicates statistical significance at greater than the 95% (light) or 99% (dark) levels based on a *t*-test, and the number of degrees of freedom is reduced based on serial correlations (Quenouille, 1954). This calculation attempts to assess whether there is greater persistence in air temperature anomalies when soil moisture is interactive (COU) than when it is fixed (OCN). Autocorrelations generally loose their significance by 3 months in both the COU and OCN simulations, so on the seasonal time scale, the differences are negligible. Examining longer lags, there are significant correlations between air temperature during March and 7–10 months later in COU (Fig. 3A), but this feature is not present in the OCN (Fig. 3B) autocorrelations. The winter-to-winter variability is the primary focus of this paper so it will be discussed in greater detail. There are other striking features in Fig. 3A such as the strong positive autocorrelations between summer air temperatures and those 12 months later. A composite analysis based on August–September land surface temperatures in eastern North America suggests that when large

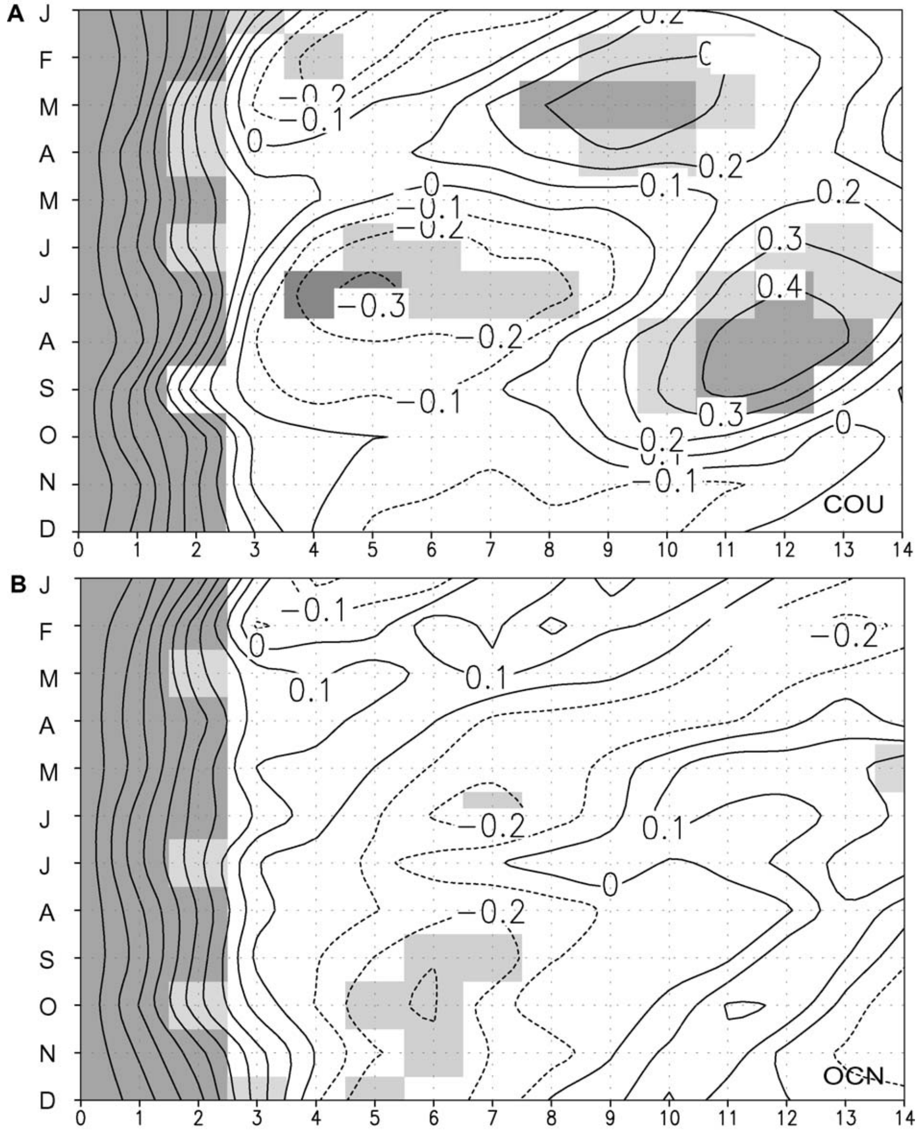

Fig. 3. Autocorrelations of an area averaged index over North America (30–45°N and 90–75°W) of 1000 mb air temperature starting from January to December and lagged up to 14 months. Autocorrelations are presented for (A) COU and (B) OCN simulations. Shading signifies statistical significance at 95% (light) and 99% (dark) levels based on a *t*-test.

negative precipitation anomalies in January and February dry the soil the following August, the persistently dry soil leads to an anomalously warm surface. This is consistent with a study by Huang et al. (1996), which found that air temperature and soil wetness are negatively correlated during the summer. The following January and February are also characterized by reduced rainfall, and the next August surface temperatures are also warm with reduced soil wetness. The question of why precipitation would be similar from one winter to the next may be related to persistent SST anomalies in the equatorial and north Pacific. Further analysis is necessary to elucidate the mechanisms related to this feature and is beyond the scope of this study. One final feature stands out in Fig. 3A; the significant negative correlations between June–July air temperature and those 4–7 months later. During the warm months, soil wetness anomalies persist for at least 5 months (see Fig. 11), and starting from a state of excess moisture during summer, the surface temperature tends to be cool from evaporation. During the winter months, these positive soil wetness anomalies have a large heat capacity, prevent the surface from excessive cooling, and are associated with warmer than normal surface temperatures. Similar arguments can be used to explain the negative correlations seen 4 months after February. As the seasons change, the relationship between soil wetness and surface temperature also changes.

The first Empirical Orthogonal Function (EOF) of observed SST in the midlatitude North Atlantic is characterized by two north–south oriented centers of opposite sign (Weare, 1977; Deser and Blackmon, 1993). The first EOFs of monthly SST from COU (Fig. 4A) and OCN (not shown) are similar and compare favorably with the observed patterns. Variability in the North Atlantic is influenced by the large-scale circulation and also by propagation of oceanic anomalies from the subtropics (Hansen and Bezdek, 1996). The total variance in the first EOF of SST is 20% smaller in the OCN simulation than the COU. Autocorrelations of the Principal Component 1 (PC1) of COU and OCN (Fig. 4B), lagged from 0 to 24 months, indicate a slower decay time in COU than OCN. The autocorrelations are similar up to a lag of 2 months after which the difference begins to grow, reaching a maximum around 11 months. This suggests that variability is different between the COU and OCN simulations on interannual time scales. Plots (similar to Fig. 3) of monthly PC1 autocorrelations show that the persistence is enhanced most in COU during the spring and summer months and least during the winter months as compared to OCN.

To examine interannual variability, in particular, the evolution of climate anomalies from one winter to the next, correlations were calculated between March surface temperature and temperature at the same grid point at various monthly lags. Significant autocorrelations between sea surface temperature during late winter and those the following winter are evident in both the COU and OCN simulations; however, the strength of these correlations is smaller in the OCN case. Autocorrelations between March surface temperature and those of the following February at the same model grid point are shown in Figs. 5 and 6 for COU and OCN, respectively. Autocorrelations for October, December, and January are displayed in Figs. 5 and 6 of Bhatt et al. (2002). In the COU simulation, the correlations drop off quickly over land and are near zero over both the midlatitude ocean and land by July. In September and October, positive correlations appear over southeastern United States and begin to increase so that by December, the lag correlations are significant over the eastern US and the western Atlantic. The correlations continue to grow over the ocean, peaking in February (Fig. 5), and then decrease fairly quickly. The correlations begin to weaken over land in February. These correlations hint at the possibility that there is some memory in the climate system in either the land and ocean system or both. In the OCN simulation, significant lag correlations in the west Atlantic Ocean appear during early winter but weaken quickly compared to COU. In addition, significant autocorrelations are not present over the land portion of the OCN simulation during any of the months of the following winter. Significant autocorrelations are present over the ocean in both of the cases but they cover a larger area in the COU simulation. One of the areas with large contrast between the COU and OCN case correlations is in the western North Atlantic, highlighted by a box (35–45°N and 75–55°W) outlined in black in Figs. 5 and 6. The differences between COU and OCN are negligible poleward of 50°N in the North Atlantic.

These results are consistent with the notion that the reemergence mechanism is operating in the COU and OCN simulations and it appears that it is weaker in OCN. Next, subsurface ocean temperature anomalies in the western North Atlantic, where the differences between COU and OCN are largest, are examined to better understand the surface climate anomalies.

3.3. Winter-to-winter climate variability

3.3.1. Ocean component

Variability within the box (35–45°N and 75–55°W) outlined in Fig. 6, where the COU and OCN differences are the largest, is compared through area averaged indices of climate variables. An index of SST was autocorrelated starting from all months and using time lags of 0–14 months (Fig. 7). On the seasonal time scale, the difference between OCN and

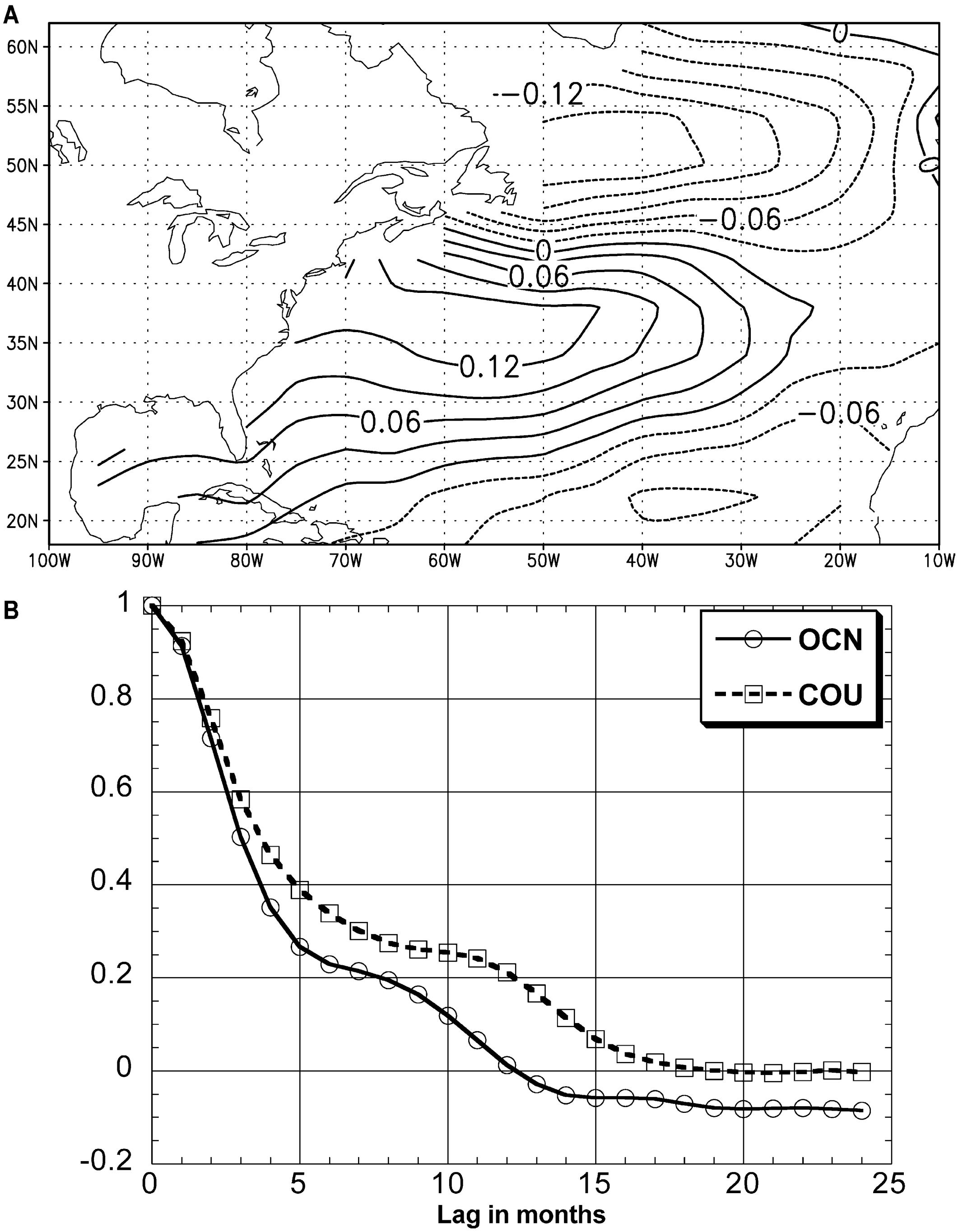

Fig. 4. EOF1 of monthly SST from the COU simulation (panel A) displayed in arbitrary units explains 19% of the variance. Monthly autocorrelations lagged up to 24 months of PC1 (panel B) of SST from COU (dashed line) and OCN (solid line) simulations. Correlations larger than approximately 0.12 are statistically significant at 95% or greater level based on a *t*-test.

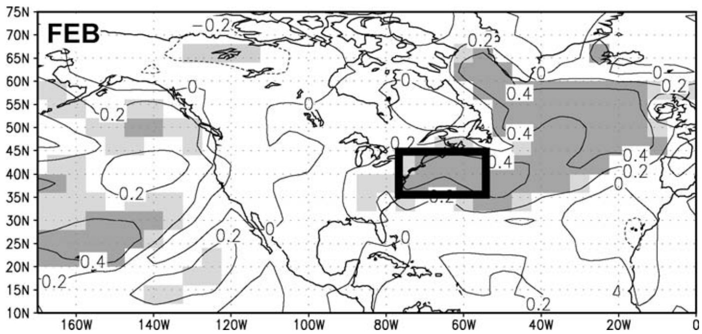

Fig. 5. Autocorrelations of March surface temperature with those at the same grid point during the following February for the COU simulation. Shading signifies statistical significance at 95% level or greater based on a *t*-test. The box outlines the region between 35–45°N and 75–55°W to highlight the domain where the differences in autocorrelation are largest between a coupled atmosphere–ocean simulation with and without an active land model.

COU is very small but, on the interannual time scale, the winter-to-winter correlations are stronger in the COU simulation (Fig. 7A and B). This is consistent with the results of Figs. 5 and 6, and the structure of these correlations has the signature of the reemergence mechanism. While these surface correlations suggest that the reemergence mechanism is weaker in the OCN simulation, analysis of subsurface anomalies is necessary.

Ocean temperatures from the surface to a depth of 245 m were spatially averaged over the box highlighted in Fig. 6. Regressions of ocean temperatures from the surface to a depth of 245 m at lags of 0–14 months on January–March seasonally averaged SST are shown in Fig. 8. The significance of the regressions was calculated using the ANOVA method (see p. 165 in Wilkes, 1995). Regression analysis patterns resemble correlation patterns but can be more insightful since one is able to compare magnitudes of anomalies. Their usefulness can be explained as follows. In July at 140 m depth, Fig. 8A and B displays approximately 0.8 and 0.7 °C/°C, respectively. This means that, for a January–March averaged SST anomaly of 1 °C, there is an anomaly of 0.8 °C in COU and 0.7 °C in OCN during July at 140 m. In both panels of Fig. 8, the regressions are fairly large at lag 0, consistent with a deep, weakly stratified late winter ocean mixed layer. The regressions at the surface drop off during the summer months when the stable upper mixed layer is decoupled from existing temperature anomalies at depth. The surface regressions increase in fall and peak in winter as the mixed layer deepens in the fall and entrains water from below. The regressions during the following

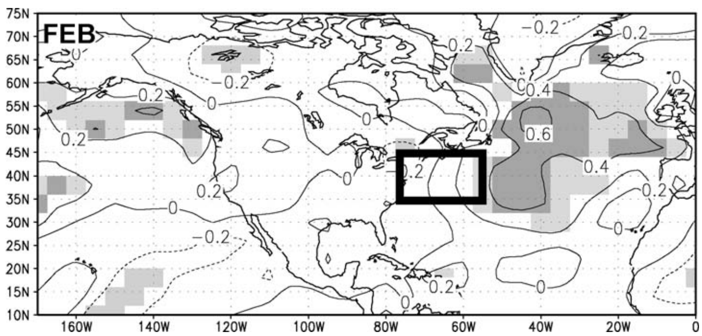

Fig. 6. Autocorrelations of March surface temperature with those at the same grid point during the following February for the OCN simulation. Shading signifies statistical significance at 95% level or greater based on a *t*-test. The box outlines the region between 35–45°N and 75–55°W to highlight the domain where the differences in autocorrelation are largest between a coupled atmosphere–ocean simulation with and without an active land model.

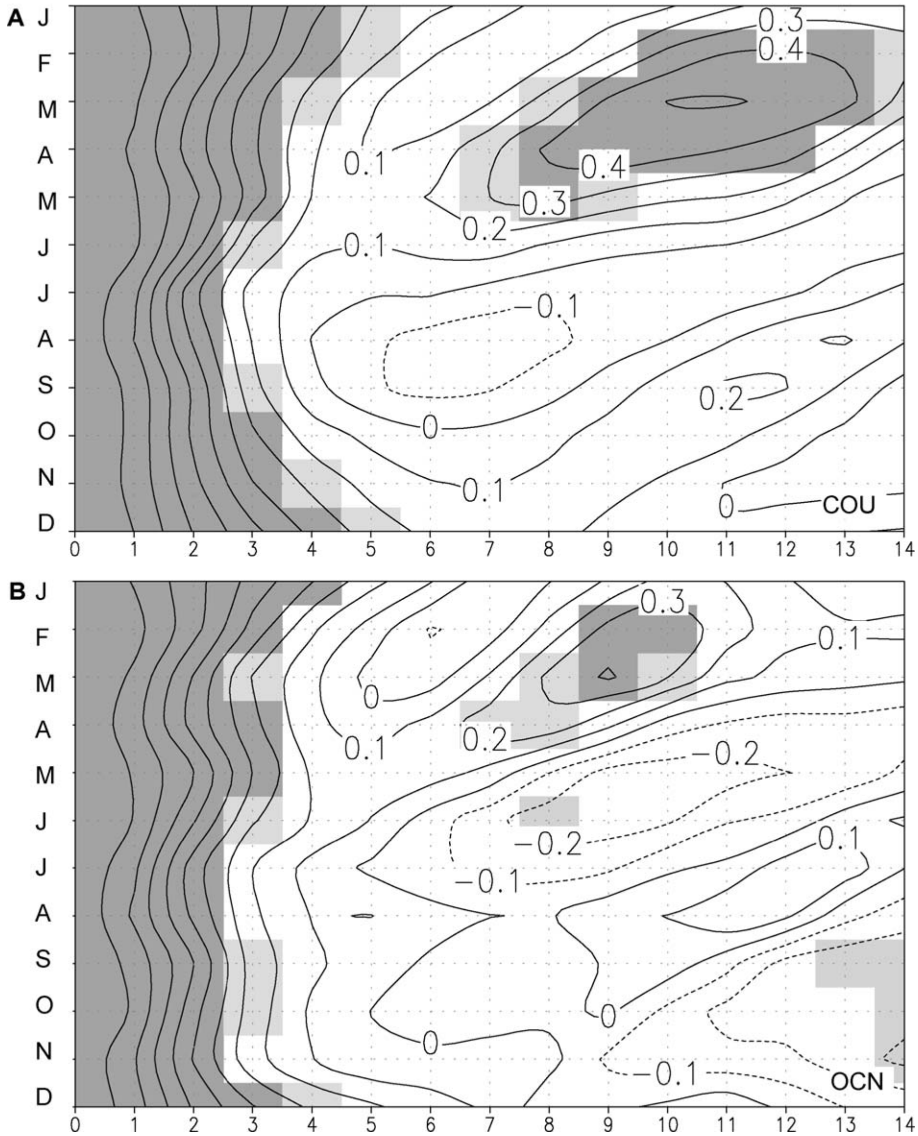

Fig. 7. Autocorrelations of an area averaged SST index (35–45°N and 75–55°W) starting from January to December lagged up to 14 months from (A) COU and (B) OCN simulations. Shading signifies statistical significance at 95% (light) and 99% (dark) levels based on a *t*-test. The area used for the index is outlined by the rectangles in Figs. 5 and 6.

winter are stronger for COU than OCN, as expected from the SST correlations. In the COU simulation, the significant regressions (>0.2 °C/°C) are larger and more long-lived than those from the OCN simulation which weaken to less than 0.2 °C/°C by early winter. Regression analysis using model data at individual grid points in this region yields similar results. At grid points farther north (e.g. 50°N and 40°W), COU and OCN reemergence strength is nearly indistinguishable, which is consistent with the autocorrelations of SST shown in Figs. 5 and 6.

Composites of temperature were constructed in order to better view the evolution of anomalies in the ocean. If departures were greater/less than +1/−1 sigma of January to March averaged SST in the west Atlantic box, then those winters were used to con-

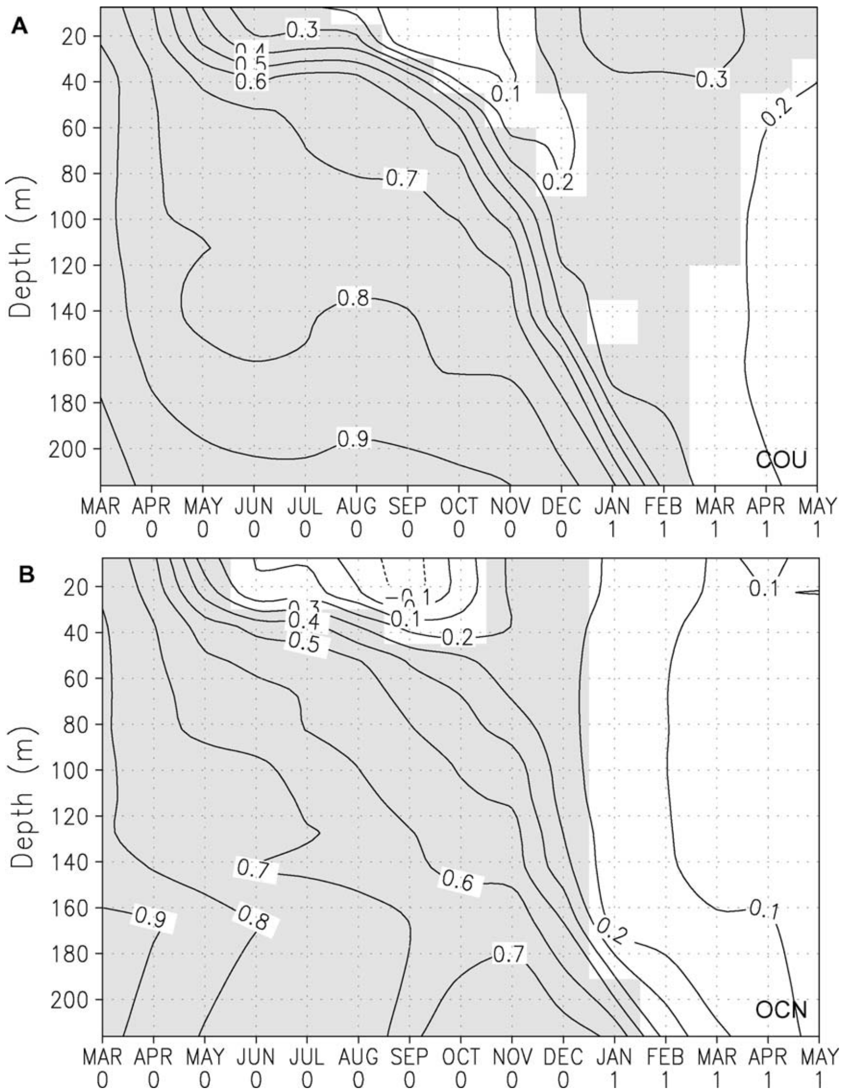

Fig. 8. Regressions of monthly ocean temperature from the surface to a depth of 245 m on January–March averaged surface ocean temperature from (A) COU and (B) OCN simulations. The regressions are based on model data averaged over the area 35–45°N and 75–55°W at lags of 0 to 14 months. Shading signifies statistical significance at 95% or greater level based on an ANOVA test. C.I. is °C/1°C^{-1}.

struct the peak season (Y0) composite. Enhanced composites, defined as positive minus negative cases, are presented for various climate variables. Significance is evaluated using a pooled variance *t*-statistic. The COU composite consists of 13 positive and 13 negative cases, whereas the OCN composite consists of 8 positive and 9 negative cases. Composites were constructed for 3-year periods, starting with one before (Y − 1) and one after (Y + 1) the peak (Y0) anomaly winter. The first and final years of the model record were excluded from being extreme winters since it is not possible to construct 3-year composites centered on the first or last model year.

The enhanced composites of ocean temperature, defined as positive minus negative cases, are shown in Fig. 9 for COU and OCN. The peak winter anomalies are stronger in the COU simulation. In the COU simulation, the subsurface anomalies persist for nearly

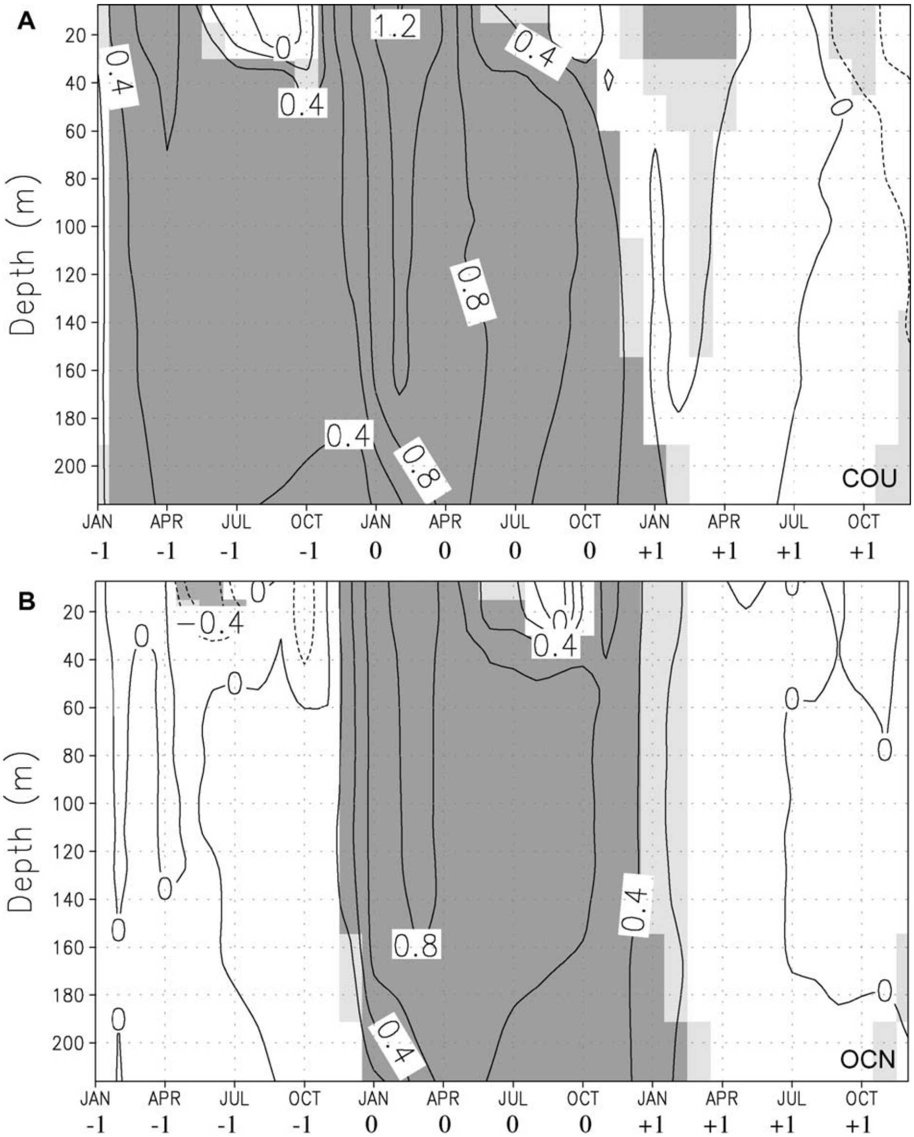

Fig. 9. Enhanced composites (positive minus negative cases) for (A) COU and (B) OCN ocean temperature with depth based on January–March averaged ocean surface temperature extremes greater than 1 sigma. The analysis is performed on area averaged ocean temperatures from 35–45°N, 75–55°W (box shown in Fig. 6). Shading signifies statistical significance at 95% (light) and 99% (dark) levels based on a pooled variance *t*-statistic.

three winters, with strong anomalies during the first two winter seasons and weaker ones during the third. In the OCN simulation, there are significant anomalies from the peak winter to the following winter. In the COU simulation, the winter before (Y − 1) the peak displays stronger anomalies than the winter after (Y + 1), whereas in OCN, it is the winter after the peak (Y + 1) that displays strong anomalies.

The ratio of the COU/OCN standard deviation of ocean temperature indicates that the COU variance is 2–4 times larger than that in OCN in most months of the year in the upper ocean mixed layer (Fig. 10). The

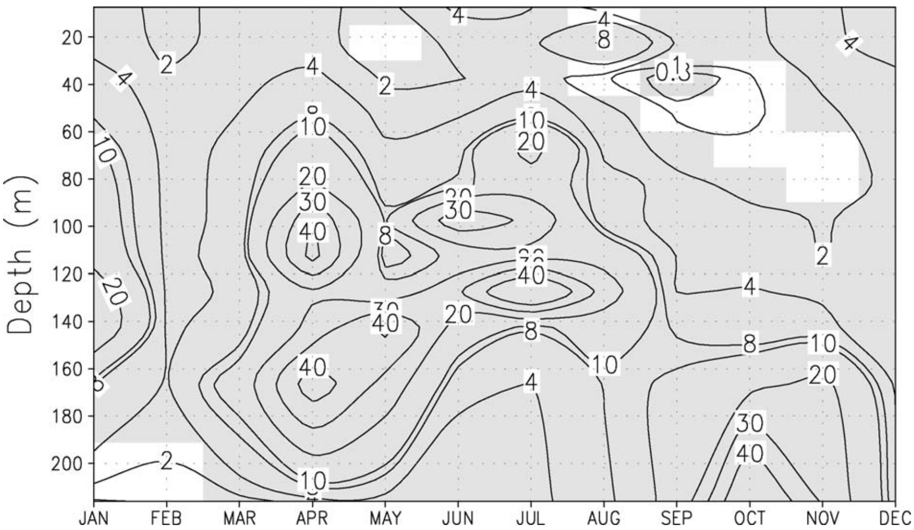

Fig. 10. Ratio of COU/OCN standard deviation of ocean temperature from the surface to a 249-m depth during each month in the area average box 35–45°N and 75–55°W. Shading signifies statistical significance at 95% level or greater based on an *f*-test.

standard deviation ratio is even larger below the mixed layer, reaching values of 40 or greater. The one exception is during September when at about 40 m depth, the standard deviation is 20% weaker in COU than OCN. Note that the influence of the midlatitude atmosphere is likely only part of the explanation for the larger variance in COU. The larger variance in the upper ocean in COU can be reasonably attributed to midlatitude processes. Some of the enhanced variability below the mixed layer is possibly associated with the larger COU anomalies penetrating to great depth during the winter. However, it is likely that part of the increased variability at depth in the ocean is associated with anomalies advected from the tropics, where the suppression of land interactions significantly reduced atmospheric variability. It is not possible to separate these effects in the present simulations.

These results are consistent with the idea that the reemergence mechanism is weaker in the OCN simulation than the COU. The midlatitude atmosphere displays higher variability which, in turn, increases the variance of the forced ocean, but it is possible that the stronger reemergence in the COU simulation results from initially larger anomalies that do not decay as quickly and are able to overcome unfavorable atmospheric forcing the following winter. To address what role the atmosphere may play in aiding reemergence, we examine the large-scale atmospheric anomalies associated with the area averaged SST index in the western North Atlantic.

3.3.2. Land component

A total soil wetness index from COU was constructed for eastern North America (30–45°N and 90–80°W) over the same region as the 1000 mb temperatures in Fig. 3. The soil wetness displays fairly long persistence during the springtime, of up to 11 months starting in April and May anomalies. The long persistence of springtime anomalies is consistent with earlier observational and modeling studies. Fig. 11 displays monthly autocorrelations for total soil wetness, and the correlation pattern is indistinguishable from that of deep soil wetness. In the OCN simulation, this low frequency component is not present as the topsoil layer is only 2 cm deep compared to the total soil layer which is ~3.5 m deep. The structure of the autocorrelations is quite complex. The significant positive correlations between September and July are consistent with the summer to summer correlations seen in surface and near surface air temperatures seen in Fig. 3A, a topic not explored in this paper. The March-to-March correlations display the signature similar to the oceanic reemergence mechanism, suggesting the possibility of a land–ocean feedback. For our purposes, the long persistence in springtime soil wetness is the key feature in Fig. 11 that can explain winter-to-winter

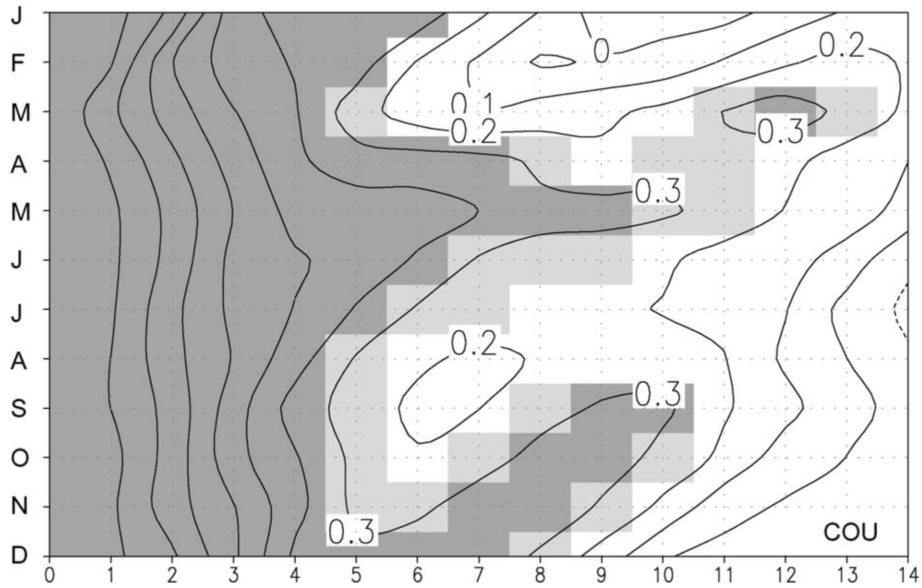

Fig. 11. Autocorrelations of an area averaged total soil wetness index over North America (30–45°N and 90–75°W) starting from January to December at lags from 0 to 14 months. Autocorrelations are presented for the COU simulation. Shading signifies statistical significance at 95% (light) and 99% (dark) levels based on a *t*-test.

persistence seen in the land surface and atmospheric temperatures.

Composites based on the same extreme seasons used to construct Fig. 9 were made for key atmospheric variables for the COU and OCN simulations, starting from January of the year before the peak up to December of the year after the peak anomaly. Select months during the 3-year period of the enhanced composites for surface temperature, sea level pressure, and total soil wetness are presented in Figs. 12–14, respectively.

During the year before the peak (Y – 1) in COU, warm anomalies are weak in January, grow in strength over the next couple of months, and then weaken in April. February Y – 1 is shown in Fig. 12A and the pattern is representative of 2 months that follow, namely March and April. The positive anomalies are gone in both the ocean and atmosphere by June, and the summer months are characterized by weak negative anomalies as can be seen during August Y – 1 (Fig. 12B). Warm anomalies are present again in November Y – 1 (Fig. 12C), grow during the next few months, and are as large as 2.5 °C in January Y0 (Fig. 12D). Significant anomalies persist in the western Atlantic until April. Land temperature anomalies are negative during the summer, peaking in September and in the fall of Y0, there are scattered positive anomalies over land and in the ocean. During the winter of Y + 1, there is an east–west band of positive SST anomalies >0.5 °C off the coast of Newfoundland. July–September of Y + 1 displays strong negative temperature anomalies over land. By the fall of Y + 1, there are negligible areas of significant positive SST anomalies. The 1000 mb air temperature has a similar evolution to the surface temperature in the composites and composites of 1000 mb specific humidity resemble those of air temperature as might be expected.

During the year before the peak (Y – 1) in OCN, there are warm anomalies over land in January and February (Fig. 12E) but no significant SST anomalies in the western Atlantic. During the summer of Y – 1, there are negative anomalies in northeastern North American and in the ocean near Newfoundland and positive anomalies in western North America (Fig. 12B). Warm anomalies appear over the southeastern US in November Y – 1 (Fig. 12G) and cover the entire US during December Y – 1 and January Y0 (Fig. 12H). Positive anomalies persist over the land until March Y0 and over the ocean until April Y0. Anomalies of both signs appear over land during the

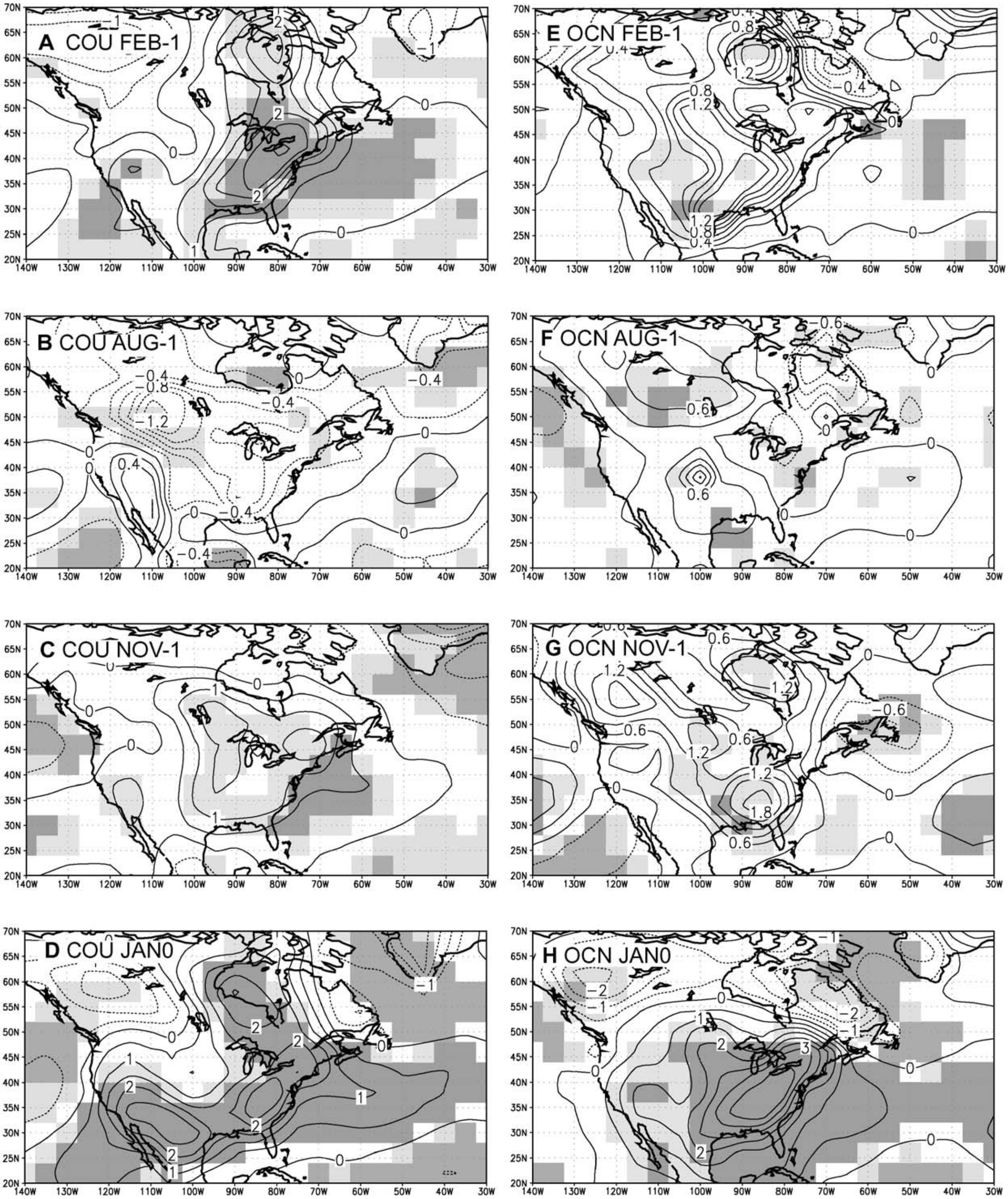

Fig. 12. Enhanced composites (positive minus negative cases) for (A–D) COU and (E–H) OCN surface temperature based on January to March averaged SST index (35–45°N and 75–55°W) extremes greater than 1 sigma during key months (Feb.-1, Aug.-1, Nov.-1 and Jan.0). Shading signifies statistical significance at 95% (light) and 99% (dark) levels based on a pooled variance *t*-statistic.

summer of Y0. Positive anomalies appear in the western Atlantic in October Y0 and over land in November Y0. Over land, the anomalies are negative by December Y0 and remain cool until April Y + 1. There are positive SST anomalies in an east–west band off the coast of Nova Scotia which remain until May Y + 1. Anomalies in the rest of Y + 1 do not resemble the patterns of interest. The 1000 mb air temperature and specific humidity composites resemble those of surface temperature, as expected.

The key difference between the two simulations is that temperature anomalies over both the land and ocean are strong during two consecutive winters in COU and only one in OCN. Additionally, these anomalies vary more smoothly in COU than OCN. The size of the temperature anomalies over land in January Y0 is actually larger in the OCN simulation than the COU. However, if a seasonal average is taken of the anomalies, those from COU are larger since they persist and do not change signs rapidly.

Sea level pressure composites are characterized by a high pressure anomaly to the north of the positive SST anomaly in the Atlantic, and the pressure is lower than normal over the North American continent. In COU, this anomaly pattern is present during January Y − 1 (Fig. 13A), is not seen in the warmer months for Y − 1, and reappears in December Y − 1 (Fig. 13B) and peaks in January Y0 (Fig. 13C). The anomaly pattern weakens and then does not appear in any substantial form in the remaining months of Y0 or Y + 1. In OCN, the anomalies are only present during the winter of the peak SST anomaly and are not present during the previous winter as seen in the plot of February Y − 1 (Fig. 13D). The anomaly is strongest in December Y − 1 (Fig. 13E) and is also present during January Y0 (Fig. 13F). Also, this pattern is not present in the remaining composite months of Y0 and Y + 1 in OCN.

This pattern of air–sea variability in the North Atlantic has been documented in the observations by Wallace et al. (1990) and is characterized by an anomalous high in SLP north of warm SST anomalies in the western Atlantic. The anomalous high is consistent with weakening westerlies and reduced advection of cold continental air over the western Atlantic and forces warm SST anomalies. The appearance of this pattern 2 years in a row in COU and only one winter in OCN suggests the possibility that once the anomalies are forced the first winter, the reemerging land and ocean anomalies favor these SLP patterns during the second winter. The warmer land may reduce the east west temperature contrast that weakens the west coast ridging (− SLP anomalies) and the east coast trough (+ SLP anomalies). During winter Y − 1, there are significant SLP anomalies in the midlatitude north Pacific, whereas during winter Y0, the largest anomalies in SLP are over North America. This is consistent with the idea that the reappearance of land and ocean anomalies acts to reinforce this pressure pattern which forced the ocean anomalies in the first place. Similar composites of SLP were constructed for a simulation not discussed in this document, which had an active land model but no ocean model (LAN). For the LAN simulation, SLP anomalies are present during the peak winter but not for either the previous or following winters. This suggests that both the ocean and atmosphere are needed to favor the appearance of this SLP pattern for two winters in a row.

The idea of the ocean anomalies reemerging has been well documented in the observations and models but a similar mechanism in the soil is not as well understood. Total soil wetness composites are shown in Fig. 14 for February Y − 1 and January Y0, and an anomalous soil wetness of + 2% to 8% is seen in both maps. The persistence of the soil wetness is critical for explaining why the temperature anomalies could be warm two winters in a row. Positive soil wetness anomalies persist over North America poleward of 35°N during the summer of Y − 1. There are negative anomalies south of 35°N but by the following winter, the demarcation between the positive and negative anomalies has shifted equator ward to 30°N (Fig. 14B). This soil wetness anomaly pattern weakens by summer Y0. In the enhanced composites of precipitation (not shown), there are significant positive rainfall anomalies over North America during February–March Y − 1 and again during January–February Y0. During the summer months and in the year after the peak winter (Y + 1), the anomalies are fairly weak. The rainfall during the first winter causes the positive soil wetness anomalies which persist long enough to favor warm surface temperatures the following fall. The warmer than normal continental mass could help maintain lower pressure over North America the next winter which would favor more precipitation, which would help maintain the positive soil

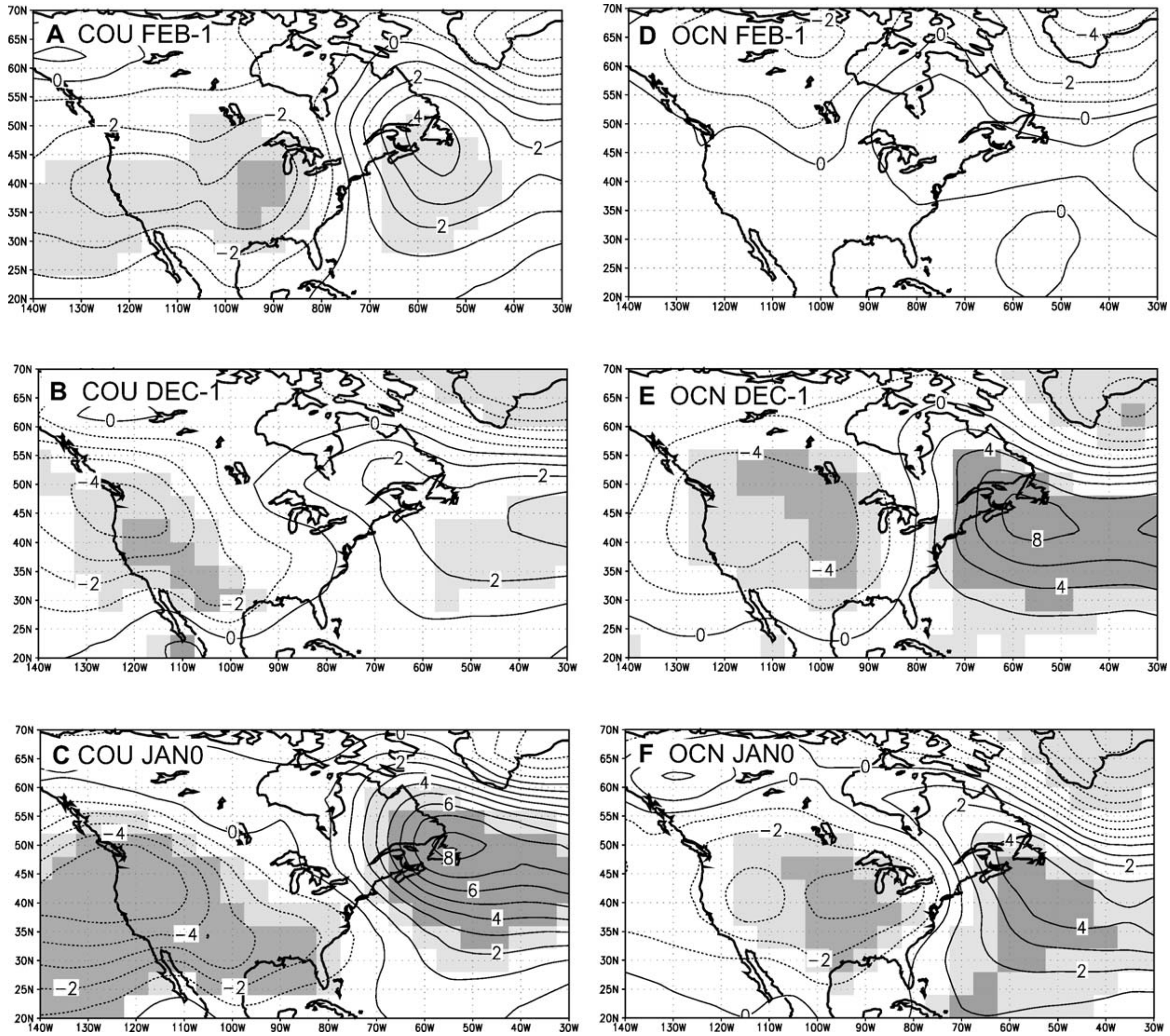

Fig. 13. Enhanced composites (positive minus negative cases) for (A–C) COU and (D–F) OCN sea level pressure based on January–March averaged SST index (35–45°N and 75–55°W) extremes greater than 1 sigma during key months (Feb.-1, Dec.-1, and Jan.0). Shading signifies statistical significance at 95% (light) and 99% (dark) levels based on a pooled variance t-statistic.

wetness anomalies. Composites of snow depth display lower than normal snow cover between 30°N and 50°N during Y − 1 and Y0 winters in both simulations, which is consistent with the warmer than normal surface temperatures.

3.3.3. Land–atmosphere–ocean

Composites of monthly anomaly indices were constructed using the same criteria as in earlier composite plots, over the land (30–45°N and 90–80°W) and ocean (35–45°N and 75–55°W) areas. Bar charts showing the evolution of heat flux components, surface temperature, and air temperature for COU and OCN highlight the differences already noted in the x–y composites discussed above. The evolution of these variables is described here and the plots are contained in Figs. 15 and 16 of Bhatt et al. (2002).

Over the eastern USA, land surface and air temperature anomalies vary together in both COU and OCN, with air temperature anomalies being slightly larger.

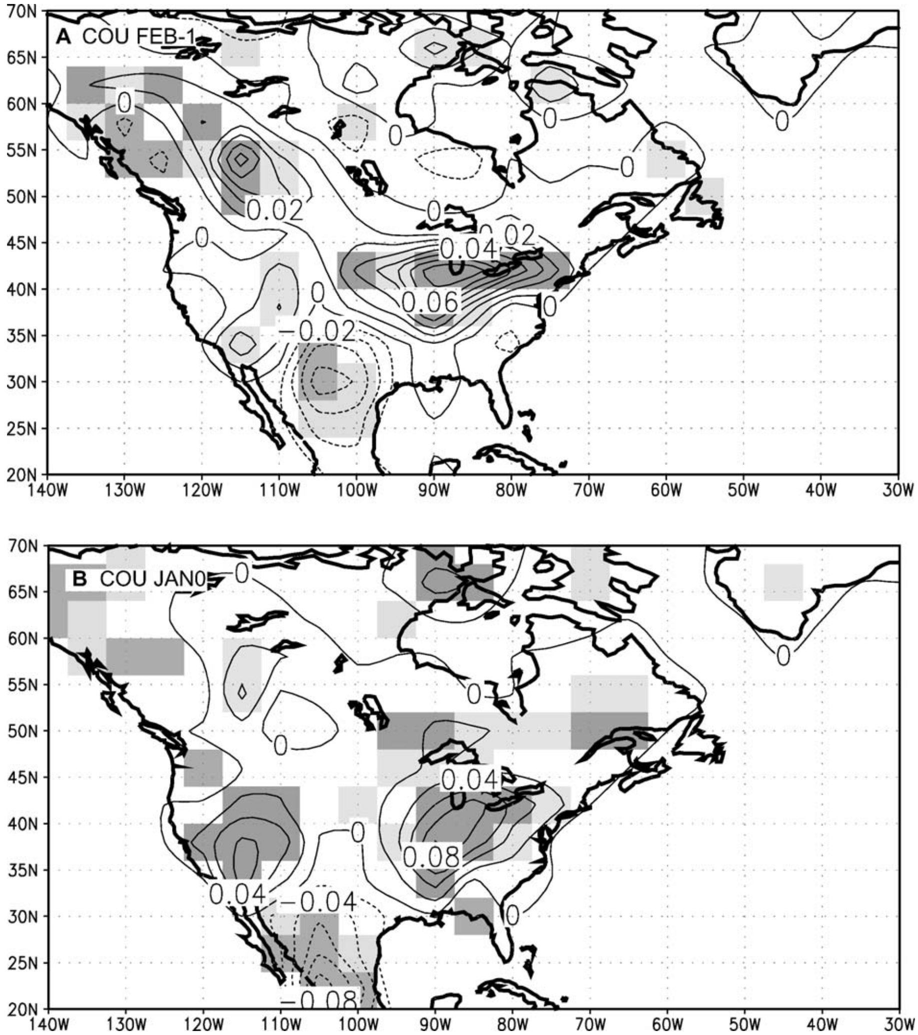

Fig. 14. Enhanced composites (positive minus negative cases) for COU total soil wetness during (A) Feb.-1 and (B) Jan.0 based on January–March averaged SST index (35–45°N and 75–55°W) extremes greater than 1 sigma. Shading signifies statistical significance at 95% (light) and 99% (dark) levels based on a pooled variance *t*-statistic. Units are % $\times 10^{-2}$ and C.I. 2%.

Warm temperature anomalies are present during November Y − 1 to March Y0 in both COU and OCN, with OCN containing the larger anomalies. The key difference between COU and OCN is the presence of large temperature anomalies during January to April Y − 1 in COU and not OCN. Temperature anomalies during January to March Y + 1 are weakly negative in both simulations. OCN heat fluxes are notably larger during January–February Y − 1 than those of COU, consistent with the larger surface temperature anomalies. During January–February Y − 1, the net heat flux is larger in COU than OCN, consistent with the warmer temperatures. During the warmer months of Y − 1, Y0, and the months of Y + 1, the net flux anomalies are weakly positive or negative. To reiterate, the key difference between the two simulations is that, in COU, there are two consecutive warm winters where anomalies last for 4–6 months, whereas in OCN, there is only one significantly anomalous winter.

During January–March of Y0, SST and near surface air temperatures are warmer than normal, with air temperature anomalies being larger. This is consistent with the heat flux anomalies which are large and positive in both OCN and COU during the peak SST anomalies. Similar to the temperature anomalies over land, it is clear that the positive SST anomalies are present over two seasons (Y − 1 and Y0) in COU and over only one second season (Y0) over OCN. But in contrast to anomalies over land, the size of the temperature anomalies is larger in COU than OCN. In general, the flux anomalies in the ocean are dominated primarily by latent followed by sensible heat flux. During November Y − 1 to February Y0, the net positive heat flux anomalies are larger in OCN but last for fewer months. During January to March Y − 1, the positive net heat flux anomalies are larger in COU than OCN. From this analysis, it is seen that the flux and temperature anomalies vary more smoothly in COU than OCN, as mentioned earlier.

The overall picture that emerges from the evidence is summarized in the schematic shown in Fig. 15 for the positive phase discussed here. The initial forcing by the atmosphere during winter is characterized by wetter than normal conditions, lower than normal pressure, warmer surface temperature, and reduced sensible and latent heat fluxes over the North American landmass. The conditions over the contiguous ocean are such that a high pressure anomaly to the north weakens the mean westerlies, reducing the advection of comparatively colder continental air over the ocean and that air which is advected is warmer than normal because of the warmer conditions over the land. This atmospheric pattern forces reduced latent and sensible heat fluxes out of the ocean and results in warmer than normal SST. The anomalies in the subsurface ocean persist throughout the summer and when the mixed layer deepens in the fall, they mix with the upper ocean and reemerge. Anomalies in deep soil moisture persist for several months after spring and favor warmer surface conditions in the subsequent fall. The reemergence of anomalies in both the land and ocean appear to work together to enhance the likelihood that a second winter will have similar climate anomalies.

4. Conclusions

A set of numerical simulations has been designed and conducted to evaluate the influence of coupled land–atmosphere and ocean–atmosphere interactions on internal climate variability. The baseline experiment was a long integration of a state-of-art coupled atmosphere–ocean–land general circulation model (COU). A sensitivity experiment was performed, where atmosphere and ocean models were interactive but the land model variability was suppressed (OCN) by specifying a fixed annual cycle of soil wetness in the lower two of three model soil layers. In this research, we focus our analysis on understanding the differences in internal climate variability between

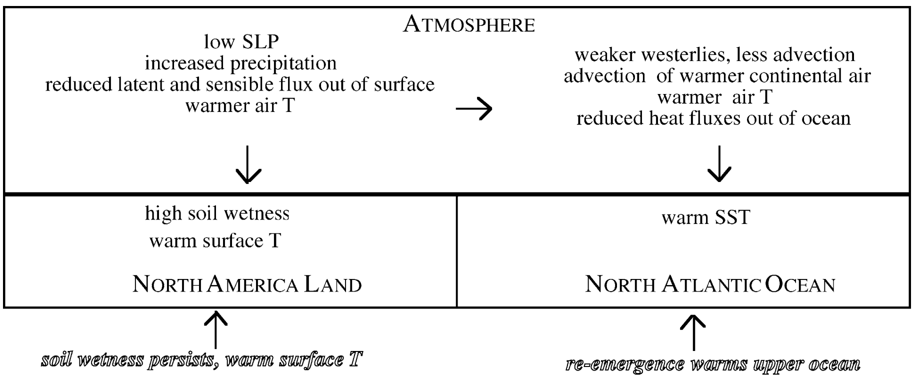

Fig. 15. Schematic outlining interaction between the land–atmosphere–ocean system in the North American–Atlantic sector. The standard font describes the conditions and interactions during winter Y − 1 and Y0, whereas the components in outlined writing occur only during Y0. The anomalies are in part able to persist because the subsurface soil wetness and subsurface ocean have been preconditioned by the anomalies from the winter Y − 1.

COU and OCN that result from including the effects of deep soil moisture in one and not the other simulation.

The variability of atmospheric air temperature as well as surface temperature is significantly reduced over North America throughout the year in the simulation where soil moisture variability has been prescribed (OCN). This reduction of air temperature variability acts to reduce ocean temperature variability in the western North Atlantic, which is strongly modified by continental air originating over North America. Net heat flux variability increases over North America when the soil moisture is prescribed, which is consistent with the idea of 'decreased thermal damping'. In OCN, the soil temperature is strongly constrained by the fixed soil wetness so does not equilibrate with the atmosphere and therefore responds to any atmospheric forcing with a strong heat flux damping (i.e. large heat flux anomaly).

The overall variability of North Atlantic SSTs is smaller when soil moisture is specified, with the COU EOF1 accounting for 20% more variability than EOF1 from OCN. Similarly, the first EOF of COU ocean heat content of the upper 250 m accounts for 22% more variability than EOF1 of OCN heat content. The first EOFs of SST and heat content are similar in pattern with a large center in the western North Atlantic and a center of opposite sign to the north. It is also possible that some of the reduction in the total variability of SST and heat content in the North Atlantic is associated with the suppression of tropical land processes. However, we found no significant correlations or regressions between ENSO variability and that in the western North Atlantic in our model simulations even though ENSO variability is greatly reduced in OCN.

The well-documented reemergence mechanism, where winter-to-winter ocean temperature anomalies are positively correlated, is operating in both simulations. This is not surprising since the ocean model which is identical in COU and OCN has fairly high resolution in the upper part of the ocean. The late winter temperature anomalies become decoupled from the atmosphere as they reside below the stable summer ocean mixed layer and are reentrained into the surface layer the following fall (Namias and Born, 1970, 1974; Alexander and Deser, 1995). The strength of reemergence is significantly weaker in the OCN simulation. This is in part due to the weaker ocean anomalies that are forced in OCN in the first place but also because the atmospheric forcing through the anomalous turbulent heat fluxes acts to reinforce the effects of the reemerging anomalies in COU but not in OCN.

Composite analysis of subsurface ocean temperatures, surface temperature, and sea level pressure indicates that the climate anomalies associated with warmer than normal SSTs in the west Atlantic are favored to occur two consecutive winters in COU but not in OCN. During the first winter, atmospheric circulation anomalies lead to warm land surface temperatures and enhanced precipitation over North America and warm SSTs in the western Atlantic. The soil wetness anomalies persist from late spring to fall and favor warm land surface conditions the second winter. Concurrently, ocean temperature anomalies persist from one winter to the next through the reemergence mechanism. During the second winter, positive surface temperature anomalies emerge over North America and western North Atlantic, and the accompanying SLP anomalies favor the maintenance of these anomalies. In contrast, in the OCN simulation, these patterns last for only one winter and this is likely associated with the lack of land temperature reemergence and weaker ocean reemergence in the western North Atlantic. It is curious that the atmospheric SLP anomalies are present for two winters in the fully coupled simulation, hinting at the possibility that they are being forced during the second winter by the land and the ocean anomalies.

In a recent observational study, Bradbury et al. (submitted for publication) found dry conditions during winter in the eastern United States are associated with below average air temperatures, anomalously cool SSTs near the North American coast, and SLP anomalies resembling the negative phase of the NAO. This observed relationship suggests that the differences in natural variability between the COU and OCN simulations may be more than just a model result.

It should be noted that it is also possible that the differences between OCN and COU that we see in the western North Atlantic are associated in part with tropical processes. The ENSO variability is greatly reduced in the OCN simulation and this may indirectly influence variability over the North Pacific and North America. Sensitivity experiments where the soil wetness is specified only over North America would be necessary in order to cleanly attribute the tropical effects.

These results suggest that soil moisture variability in the midlatitudes could add persistence to the climate system on interannual time scales by influencing ocean variability. Another interesting consequence of this result is the possibility that land processes could play a role in the 'atmospheric bridge', a mechanism that teleconnects North Pacific ocean temperature anomalies to the North Atlantic sector (Lau and Nath, 1996).

Acknowledgements

This research was funded by the Frontier Research System for Global Change through the IARC and the National Science Foundation ATM-9520579 and ATM-9907915. We would like to thank Paul Dirmeyer, Ben Kirtman, Sirpa Häkkinen, Tim Delsole, Phil Duffy, and the anonymous reviewers for their contributions to this work. We would like to acknowledge Brian Doty (COLA) and the GrADS community (http://www.iges.org/grads/) for providing the graphics software. U.S.B. would also like to thank Christopher Swingley of IARC/Frontier for his assistance with various computer issues.

References

Alexander, M.A., Deser, C., 1995. A mechanism for the recurrence of wintertime midlatitude SST anomalies. J. Phys. Oceanogr. 25, 122–137.

Barsugli, J.J., Battisti, D.S., 1998. The basic effects of coupling between the atmosphere and ocean in the midlatitudes. J. Atmos. Sci. 55, 477–493.

Battisti, D.S., Bhatt, U.S., Alexander, M.A., 1995. A modeling study of the interannual variability of sea-surface temperature in the wintertime N. Atlantic Ocean. J. Climate 8, 3067–3083.

Betts, A.K., Ball, J.H., Beljaars, A.C.M., Miller, M.J., Viterbo, P.A., 1996. The land-surface–atmosphere interactions: a review based on observational and global modeling perspectives. J. Geophys. Res. 101 (D3), 7209–7226.

Bhatt, U.S., Alexander, M., Battisti, D., Houghton, D., Keller, L., 1998. Atmosphere–ocean interaction in the North Atlantic: near surface climate variability. J. Climate 11, 1615–1632.

Bhatt, U.S., Schneider, E.K., DeWitt, D.G., 2002. Influence of North American Land Processes on North Atlantic SST Variability. COLA Report 112 [available from Center for Ocean–Land–Atmosphere Studies, 4041 Powder Mill Rd., Suite 302, Calverton, MD 20705-3106].

Bjerknes, J., 1962. Synoptic survey of the interaction of sea and atmosphere in the North Atlantic. Vilhelm Bjerknes Centenary Volume, Vol. XXIV. Geophys. Publ., vol. 3, pp. 115–145.

Bjerknes, J., 1964. Atlantic air–sea interaction. Adv. Geophys. 20, 1–82.

Bladé, I., 1997. The influence of midlatitude coupling on the low-frequency variability of a GCM: Part I. No tropical forcing. J. Climate 10, 2087–2106.

Bradbury, J.A., Dingman, S.L., Keim, B.D., 2002. Relation of New England hydroclimate to large-scale atmospheric circulation patterns. J. Am. Water Resour. Assoc. 38, 1287–1299.

Cayan, D., 1992. Latent and sensible heat flux anomalies over the northern oceans: the connection to monthly atmospheric circulation. J. Climate 5, 354–369.

Delworth, T., Manabe, S., 1989. The influence of soil wetness on near-surface atmospheric variability. J. Climate 2, 1447–1462.

Deser, C., Blackmon, M.L., 1993. Surface climate variations over the North Atlantic Ocean during winter: 1900–89. J. Climate 6, 1743–1753.

DeWitt, D.G., 1996. The effect of the cumulus convection scheme on the climate of the COLA general circulation model. COLA Report No. 27, 43 pp. [available from Center for Ocean–Land–Atmosphere Studies, 4041 Powder Mill Rd., Suite 302, Calverton, MD 20705-3106].

DeWitt, D.G., Schneider, E.K., 1997. Simulation of the climate with a coupled ocean–atmosphere general circulation model: seasonal cycle and adjustment to mean climate. COLA Report No. 44. [available from Center for Ocean–Land–Atmosphere Studies, 4041 Powder Mill Rd., Suite 302, Calverton, MD 20705-3106].

DeWitt, D.G., Schneider, E.K., 1999. The processes determining the annual cycle of equatorial sea surface temperature: a coupled general circulation model perspective. Mon. Weather Rev. 127, 381–395.

Duchon, C.E., 1979. Lanczos filtering in one and two dimensions. J. Appl. Meteorol. 18, 1016–1022.

Frankignoul, C., 1985. Sea surface temperature anomalies, planetary waves, and air–sea feedback in the middle latitudes. Rev. Geophys. 23, 357–390.

Hansen, D.V., Bezdek, H., 1996. On the nature of decadal anomalies in North Atlantic sea surface temperature. J. Geophys. Res. 101, 8749–8758.

Harshvardhan, Davies, R., Randall, D.A., Corsetti, T.G., 1987. A fast radiation parameterization for atmospheric circulation models. J. Geophys. Res. 92 (D1), 1009–1016.

Hasselmann, K., 1976. Stochastic climate models: I. Theory. Tellus 28, 473–485.

Huang, J., van den Dool, H.M., Georgakakos, K.P., 1996. Analysis of model-calculated soil moisture over the United States (1931–1993) and applications to long-range temperature forecasts. J. Climate 9, 1350–1362.

Kiehl, J.T., Hack, J.J., Bonan, G.B., Boville, B.A., Briegleb, B.P., Williamson, M.D.L., Rasch, P.J., 1996. Description of the NCAR Community Climate Model (CCM3), NCAR Tech. Note

NCAR/TN-420 + STR, 152 pp. [available from the National Center for Atmospheric Research, Boulder, CO 80307].

Kiehl, J.T., Hack, J.J., Bonan, G., Boville, B.A., Williamson, D.L., Rasch, P.J., 1998. The National Center for Atmospheric Research Community Climate Model: CCM3. J. Climate 11, 1131–1149.

Kinter III, J.L., Shukla, J., Marx, L., Schneider, E.K., 1988. A simulation of the winter and summer circulations with the NMC global spectral model. J. Atmos. Sci. 45, 2486–2522.

Koster, R.D., Suarez, M.J., 1995. Relative contributions of land and ocean processes to precipitation variability. J. Geophys. Res. 100 (D7), 13775–13790.

Lacis, A.A., Hansen, J.E., 1974. A parameterization for the absorption of solar radiation in the earth's atmosphere. J. Atmos. Sci. 31, 118–133.

Lau, N.-C., Nath, M.J., 1996. The role of the 'atmospheric bridge' in linking tropical Pacific ENSO events to extratropical SST anomalies. J. Climate 9, 2036–2057.

Levitus, S., 1982. Climatological Atlas of the World Ocean. NOAA Professional Paper 13. U.S. Dept. of Commerce. 173 pp.

Liu, Y., Avissar, R., 1999. A study of persistence in the land–atmosphere system using a general circulation model and observations. J. Climate 12, 2139–2153.

Mellor, G.L., Yamada, T., 1982. Development of a turbulence closure model for geophysical fluid processes. Rev. Geophys. Space Phys. 20, 851–875.

Miyakoda, K., Sirutis, J., 1977. Comparative integrations of global spectral models with various parameterized processes of subgrid scale vertical transports. Beitr. Phys. Atmos. 50, 445–447.

Moorthi, S., Suarez, M.J., 1992. Relaxed Arakawa–Schubert: a parameterization of moist convection for general circulation models. Mon. Weather Rev. 120, 978–1002.

Namias, J., 1959. Persistence of mid-tropospheric circulations between adjacent months and seasons. In: Bolin, B. (Ed.), The Atmosphere and the Sea in Motions: Rossby Memorial Volume. Rockefeller Institute Press and Oxford Univ. Press, pp. 240–248.

Namias, J., 1963. Surface–atmosphere interactions as fundamental causes of droughts and other climatic fluctuations. Arid Zone Research, vol. 20, Changes of Climate Proc. of Rome Symp. UNESCO and WMO, Paris, pp. 345–359.

Namias, J., Born, R.M., 1970. Temporal coherence in North Pacific sea-surface temperatures. J. Geophys. Res. 75, 5952–5955.

Namias, J., Born, R.M., 1974. Further studies of temporal coherence in North Pacific sea surface temperatures. J. Geophys. Res. 79, 797–798.

Pacanowski, R.C., 1995. MOM 2 documentation, user's guide and reference manual. GFDL Ocean Group Tech. Rep. No. 3, 246 pp. [available from GFDL/NOAA, P.O. Box 308, Princeton, NJ 08542].

Pacanowski, R.C., Philander, S.G.H., 1981. Parameterization of vertical mixing in numerical models of tropical oceans. J. Phys. Oceanogr. 11, 1443–1451.

Palmer, T.N., Shutts, G.J., Swinbank, R., 1986. Alleviation of a systematic westerly bias in general circulation and numerical weather prediction model through an orographic gravity wave parameterization. Q. J. R. Meteorol. Soc. 112, 1001–1039.

Quenouille, M., 1954. Associated Measurements. Butterworth, London. 242 pp.

Rind, D., 1982. The influence of ground moisture conditions in North American on summer climate as modeled in the GISS GCM. Mon. Weather Rev. 110, 1487–1494.

Rosati, A., Miyakoda, K., 1988. A general circulation model for upper ocean simulations. J. Phys. Oceanogr. 18, 1601–1626.

Saravanan, R., 1998. Atmospheric low frequency variability and its relationship to midlatitude SST variability: studies using the NCAR Climate System Model. J. Climate 11, 1386–1404.

Sato, N., Sellers, P.J., Randall, D.A., Schneider, E.K., Shukla, J., Kinter III, J.L., Hou, Y.-T., Albertazzi, E., 1989. Effects of implementing the simple biosphere model in a general circulation model. J. Atmos. Sci. 46, 2757–2782.

Schneider, E.K., Kinter III, J.L., 1994. An examination of internally generated variability in long climate simulations. Clim. Dyn. 10, 181–204.

Schneider, E.K., Zhu, Z., 1998. Sensitivity of the simulated annual cycle of sea surface temperature in the equatorial Pacific to sunlight penetration. J. Climate 11, 1932–1950.

Schneider, E.K., Zhu, Z., Giese, B.S., Huang, B., Kirtman, B.P., Shukla, J., Carton, J.A., 1997. Annual cycle and ENSO in a coupled ocean–atmosphere general circulation model. Mon. Weather Rev. 125, 680–702.

Sellers, P.J., Mintz, Y., Sud, Y.C., Dalcher, A., 1986. A simple biosphere model (SiB) for use within general circulation models. J. Atmos. Sci. 43, 505–531.

Vinnikov, K., Robuck, A., Speranskaya, N.A., Schlosser, C.A., 1996. Scales of temporal and spatial variability of midlatitude soil moisture. J. Geophys. Res. 101 (D3), 7163–7174.

Wallace, J.M., Jiang, Q., 1987. On the observed structure of the interannual variation of the atmosphere/ocean climate system. In: Cattle, H. (Ed.), Atmospheric and Oceanic Variability. Royal Meteorological Society, Bracknell, Berkshire, pp. 17–43.

Wallace, J.M., Smith, C., Jiang, Q., 1990. Spatial patterns of atmosphere–ocean interaction in the northern winter. J. Climate 3, 990–998.

Watanabe, M., Kimoto, M., 2000. On the persistence of decadal SST anomalies in the North Atlantic. J. Climate 13, 3017–3028.

Weare, B.C., 1977. Empirical orthogonal analysis of Atlantic Ocean surface temperatures. Q. J. R. Meteorol. Soc. 103, 467–478.

Wilkes, D.S., 1995. Statistical Methods in Atmospheric Sciences. Academic Press, San Diego. 467 pp.

Xue, Y., Sellers, P.J., Kinter III, J.L., Shukla, J., 1991. A simplified biosphere model for global climate studies. J. Climate 4, 345–364.